

# A Spectral Domain Decomposition Technique for Viscous Compressible Flows

S. Gauthier \*

F. Renaud \*

## Abstract

A domain decomposition method is proposed for the numerical solution of the viscous compressible time-dependent Navier-Stokes equations. The solution technique consists of a Fourier-Chebyshev collocation method combined with a patching method. The computational domain is decomposed into subdomains in the vertical direction only. The elliptic problems coming from the viscous terms are solved iteratively by means of the Chebyshev procedure. Density is matched with a simple upwind procedure, while the velocities and the temperature are handled with the influence matrix method. Numerical examples are performed on both stationary - Rayleigh-Bénard convection - and time-dependent (the so-called "mixing layer") compressible viscous flows. The method may be extended to three-dimensional flows with non-periodic directions.

**Key words:** spectral methods, domain decomposition, viscous compressible flows.

**AMS subject classifications:** 65M99, 65M50, 65M35.

## 1 Introduction

Domain decomposition methods have become popular in the last years [1]. The motivation is at least twofold. First, these methods are well suited to handle complex geometries. Second, they naturally lead to algorithms adapted to parallel computers. However, in the framework of spectral methods, there is a third motivation since domain decomposition methods are also a way to handle flows with strong gradients. In this case, the main gradients of the

flow are embedded in a subdomain that can follow the gradients. Moreover, in each subdomain, a transformation of coordinates may be used to increase the global accuracy.

The adaptive coordinate transform based on the minimization of some norms was first introduced in [2] and, independently, in [3]. In [2], a coordinate transform was chosen to minimize the weighted second Sobolev norm of the solution. The numerical method was proven to be efficient to compute steady non-axisymmetric as well as unsteady axisymmetric flames. In [3], the same norm - the weighted second Sobolev norm - was used to simulate a two-dimensional plane flame moving into a reactive medium. The histogram of the Chebyshev expansion of the solution proves that spectral accuracy has been reached.

In [4], mappings are used to solve a linear hyperbolic equation with a Fourier or a Chebyshev method. The solution obtained with a mapping adapted with the norm displayed much fewer oscillations than the solution without mapping. It turns out that the best results are obtained with the  $H^2$ -norm.

In [5] and [6], the authors compare three functionals: the weighted Sobolev norms introduced in [2] and [3], the non-weighted norm, and the functional proposed in [7]; which is an upper bound for the maximum norm of the spectral interpolation error. They found that, at least for the studied cases, the choice of a specific functional is not too critical. However, the crucial point is the actual evaluation of the functionals. They selected the best way to perform this computation. This numerical procedure is used to simulate the temporally growing compressible mixing layers.

However, such a method cannot handle several stiff gradients on the same domain : the effect of the presence of one gradient is to bring most of the collocation points in the vicinity of the strong gradient. It may result in a lack of resolution elsewhere. In other words, there is only one, or sometimes two, parameters in the mappings, making them not flexible enough for some complicated solutions. This is the reason the domain decomposition strategy may be useful in simulating these flows.

The domain decomposition strategy may be used in two ways : applying it to methods of variational type and ap-

---

\*CEA, Centre d'Études de Limeil-Valenton 94195 Villeneuve St Georges, Cédex, FRANCE

plying it to patching methods. Examples belonging to the first type are the spectral element method [8] and the method described in [9]. In these methods, one defines a large number of subdomains, with a small number of collocation points, without transformation of coordinate. The accuracy is obtained by increasing the number of subdomains rather than the number of points in each subdomain. The second type of methods - the patching methods - uses a relatively small number of subdomains with a large number of collocation points in order to reach spectral accuracy. In each subdomain, self-adaptive transformations of coordinate, which depend on one or more parameters, may be used. The values at the interfaces are solutions of a system which can be solved directly or iteratively.

The first application of a spectral multi-domain method for viscous compressible flows was presented in [10]. The method imposes a global flux balance condition at the interface. This scheme is applied to one-dimensional supersonic viscous compressible reacting flows up to Mach 11. In the middle domain, a mapping is used and the parameter is adjusted by hand.

Domain decomposition for inviscid compressible flows have been investigated by Kopriva [11], who successively studied multidomain in one and two-directions of a two-dimensional space. In the latter case, the solution in complex geometries is obtained using a combination of patched and overset grids. The extension to viscous flows is presented in [12], where a two-dimensional, nonoverlapping multidomain spectral collocation method is applied to subsonic and supersonic flows over a flat plate. In each subdomain, linear, non-adaptive transformations of coordinates are used and time marching is explicit.

In this paper, we present a multidomain patching technique for the full Navier-Stokes equations. The dependent variables are expanded on the Fourier functions in the horizontal homogeneous direction and on the Chebyshev polynomials in the vertical inhomogeneous direction. The features of our method are as follows:

1. Time marching is done with a semi-implicit third order Runge-Kutta scheme in a low-storage formulation [13], [14]. The advective terms are treated explicitly and all diffusion terms are handled implicitly. Since transport coefficients are constant, the implicit stage is performed in the Fourier space by means of a Chebyshev iterative scheme [15]. This procedure allows us larger time steps.
2. The vertical direction is decomposed into nonoverlapping subdomains. Density is matched with a simple upwind procedure. The velocities and the temperature are handled with the influence matrix method

which reflects the continuity of the function and its first normal derivative at the interface.

3. In each subdomain, a self-adaptive transformation of a coordinate is used. Indeed, since strong gradients may occur in the middle of the subdomain, a transformation of coordinate is used to bring the mesh points in the vicinity of the gradient. These mappings need to be self-adaptive because these gradients move in time. Consequently, the parameters of these mappings are recalculated frequently during the computation. This technique leads to a better accuracy. The parameters of the mappings are optimized by minimizing the  $H_{\omega}^2$  norm, as in [5].

The numerical algorithm is first tested against a steady state of the compressible Rayleigh-Bénard convection. This solution is used as a test of the multidomain method, since no strong gradients occur. Then, simulations of the time-dependent Kelvin-Helmholtz instability, in which strong gradients occur in the middle of the central subdomain and move in time, are carried out and analyzed.

The next section recalls the basic equations. The algorithm is described in Section 3. Numerical applications are reported in Section 4.

## 2 Governing equations

We use the full Navier-Stokes equations under the form

$$(1) \quad \frac{\partial \rho}{\partial t} + \nabla_i \rho u_i = 0,$$

$$(2) \quad \frac{\partial \rho u_i}{\partial t} + \nabla_j \rho u_i u_j = -A_u \nabla_i P + B_u \nabla_j \sigma_{ij} + C_{u_i} \rho.$$

The energy equation is written for the total energy  $E$ , it reads

$$(3) \quad \frac{\partial \rho E}{\partial t} + \nabla_i \rho u_i \left( E + A_T \frac{P}{\rho} \right) = +B_T \nabla_i \nabla_i T + C_T \nabla_i (\sigma_{ij} u_j),$$

where  $\sigma_{ij}$  is the viscous stress tensor.

$$(4) \quad \sigma_{ij} = \nabla_i u_j + \nabla_j u_i - \frac{2}{3} \delta_{ij} \nabla_\ell u_\ell.$$

The system of equations is close with the perfect gas law. The thermal conductivity and the dynamic viscosity have been taken constant and the values of the constants appearing in the Eqs.(1-4) will be specified below, in the numerical applications.

### 3 The numerical method

#### 3.1 The domain decomposition method

The physical variables  $\rho$ ,  $\mathbf{u} = (u, v)^\dagger$  and  $E$  are expanded on each subdomain, on the Fourier functions in the horizontal homogeneous direction, and on the Chebyshev polynomials in the vertical inhomogeneous direction. The temporal discretization is the third order, low storage, semi-implicit Runge-Kutta scheme [13], [14]. All diffusive terms are handled implicitly in the Fourier space by means of a Chebyshev iterative procedure according to [15].

The system of the full Navier-Stokes equations is incompletely parabolic, since the equation for the density is hyperbolic. The matching of the density requires only the continuity of the function. A simple scheme for this reads

$$(5) \quad \begin{aligned} \rho(z_{t,s}) &= (1 - \eta) \rho_s(z_{t,s}) + \\ &\quad \eta \rho_{s+1}(z_{b,s+1}) \text{ if } v < 0 \\ \rho(z_{t,s}) &= \eta \rho_s(z_{t,s}) + \\ &\quad (1 - \eta) \rho_{s+1}(z_{b,s+1}) \text{ if } v > 0 \\ &\text{for } s = 1, \dots, S - 1, \end{aligned}$$

where  $z_{t,s}$  (resp.  $z_{b,s}$ ) is the upper coordinate (resp. lower) of the interface of the subdomain  $s$ , and  $S$  is the total number of subdomains. The parameter  $\eta$  is a real number between 0 and 1. The value  $\eta = 1$  corresponds to a pure upwind scheme. In this case, the density equation is solved in the subdomain number 1, without boundary conditions. In the second domain the equation is solved by using the value of the density of the previous domain, at the interface, as a boundary condition. For any value different from  $\eta = 1$ , Eq.(5) is an averaging procedure between two adjacent subdomains. The parabolic equations require the matching of the function and its first derivatives. Several solution techniques are available (for a review, see [13]) and we chose, for the simulations reported here, the influence matrix technique used in the domain decomposition framework in [16] and [17]. Since all diffusive terms in the full Navier-Stokes equations are nonlinear, these terms are separated into two contributions as

$$(6) \quad \frac{1}{\rho} \frac{\partial \sigma_{ij}}{\partial x_j} = \left( \frac{1}{\rho} - \frac{1}{\rho_s} \right) \frac{\partial \sigma_{ij}}{\partial x_j} + \frac{1}{\rho_s} \frac{\partial \sigma_{ij}}{\partial x_j},$$

where  $\rho = \rho(x, z, t)$  and  $\rho_s = \rho_s(z)$ . This does depend upon the  $z$ -coordinate and thus may be close to the total density. The difference between  $\rho - \rho_s$  is only due to the variation of the density in the  $x$ -direction. The first part is treated explicitly, while the second is handled implicitly. This splitting has been suggested in [18] and used by several authors [19].

The matrix influence method is applied to the temperature and to the two components of the velocity. The method for a scalar variable is given in [16] and in the latter case, it is generalized as follows. The solution is decomposed as

$$(7) \quad \begin{aligned} \mathbf{u}^s &= \bar{\mathbf{u}}^s + \lambda_1^s \mathbf{u}_1^s + \lambda_2^s \mathbf{u}_2^s \\ &+ \lambda_3^s \mathbf{u}_3^s + \lambda_4^s \mathbf{u}_4^s \text{ for } s = 1, \dots, S \end{aligned}$$

The  $\lambda_p^s$  are real coefficients which have to be determined with the continuity conditions. The velocity  $\bar{\mathbf{u}}^s$  is the solution of a non-homogeneous elliptic problem

$$(8) \quad \begin{aligned} \frac{d^2 \bar{u}^s}{dz^2} - \sigma_{,u} \bar{u}^s - \kappa_{,u} \frac{d\bar{u}^s}{dz} &= S_{,u}, \\ \frac{d^2 \bar{v}^s}{dz^2} - \sigma_{,v} \bar{v}^s - \kappa_{,v} \frac{d\bar{v}^s}{dz} &= S_{,v}, \quad s = 1, \dots, S, \end{aligned}$$

with homogeneous Dirichlet boundary conditions

$$(9) \quad \bar{\mathbf{u}}^s(z_{b,s}) = 0, \bar{\mathbf{u}}^s(z_{t,s}) = 0, \quad s = 1, \dots, S.$$

The  $\mathbf{u}_p^s$  are solutions of homogeneous problems

$$(10) \quad \begin{aligned} \frac{d^2 u_p^s}{dz^2} - \sigma_{,u} u_p^s - \kappa_{,u} \frac{d u_p^s}{dz} &= 0, \\ \frac{d^2 v_p^s}{dz^2} - \sigma_{,v} v_p^s - \kappa_{,v} \frac{d v_p^s}{dz} &= 0, \end{aligned}$$

for  $s = 1, \dots, S$ , and  $p = 1, 2, 3, 4$

with non-homogeneous Dirichlet boundary conditions written as

$$(11) \quad \begin{aligned} \bar{u}_p^s(z_{b,s}) &= \delta_{1p}, & \bar{u}_p^s(z_{t,s}) &= \delta_{2p} \\ \bar{v}_p^s(z_{b,s}) &= \delta_{3p}, & \bar{v}_p^s(z_{t,s}) &= \delta_{4p} \end{aligned}$$

for  $s = 1, \dots, S$ , and  $p = 1, 2, 3, 4$

The problems defined by Eqs.(8-11) are one-dimensional, linear with variable coefficients. It is well-known that the matrix associated to this system is ill-conditioned. As a result, it is solved with the Chebyshev iterative procedure detailed in [15]. The physical boundary conditions are of the general form

$$(12) \quad \begin{aligned} \alpha_{1,u} \frac{du}{dz}(z_{b,1}) + \beta_{1,u} u(z_{b,1}) &= 0, \\ \alpha_{S,u} \frac{du}{dz}(z_{t,S}) + \beta_{S,u} u(z_{t,S}) &= 0, \end{aligned}$$

and the same set of equations for the vertical velocity. The matching conditions read

$$(13) \quad \begin{aligned} \mathbf{u}^s(z_{t,s}) &= \mathbf{u}^{s+1}(z_{b,s+1}), \quad s = 1, \dots, S - 1, \\ \frac{d\mathbf{u}^s}{dz}(z_{t,s}) &= \frac{d\mathbf{u}^{s+1}}{dz}(z_{b,s+1}), \quad s = 1, \dots, S - 1, \end{aligned}$$

Rayleigh number	$V_{max}$	$Mach_{max}$	$\rho_{max}$	$T_{max}$	$P_{max}$	$\omega_{max}$	$\omega_{min}$	$(div\mathbf{u})_{max}$	$(div\mathbf{u})_{min}$
1000	15.125	0.175	0.068	0.063	0.051	75.595	-75.595	5.141	-10.246

Table 1: Characteristics of the Rayleigh-Bénard steady solution. The Rayleigh number is equal to 1000,  $Z = 1$ ,  $m = 1$ , the Prandtl number and the adiabatic index are equal to 0.71 and 1.67, respectively. The norm of the velocity is  $V$ .  $\rho_{max}$ ,  $T_{max}$ , and  $P_{max}$  are the maximum of the relative fluctuations of the density, temperature and pressure, respectively. The vorticity is  $\omega$  and  $div\mathbf{u}$  is the divergence of the flow.

The set of Eqs.(12, 13) is a linear algebraic system of 45 equations. The resolution provides the  $\lambda$ 's that allows us to build the solution in each subdomain through Eq.(7).

### 3.2 The adaptive coordinate transform

As already stated, the representation of a strong gradient anywhere in the domain  $[-1, 1]$  requires a huge number of polynomials unless a transformation of coordinate of the form  $z = f(\xi, a)$  is used, where  $a$  is a real parameter. The physical  $z$ -space is mapped, by the function  $f$ , in the computational  $\xi$ -space. In this new space, functions which exhibit rapid variations in the physical space, have a slow variation, provided the parameter  $a$  is correctly chosen. It has been shown [2], [3] that the optimal choice is obtained by minimizing the interpolation error. This one is bounded by the norm of the solution itself through the inequality

$$(14) \quad \begin{aligned} \|u - I(u)\|_{\mu, \omega} &\leq CN^{2\mu - \sigma - 1/2} \|u\|_{\sigma, \omega} \\ \text{for } \sigma &\geq 1/2 \text{ and } 0 \leq \mu \leq \sigma. \end{aligned}$$

The inequality (14) provides a criterion to select the best value of the parameter  $a$ . The practical computation of the weighted Sobolev  $H_{\omega}^2$ -norm is detailed in [5]. The criterion applies to one variable or a combination of variables. This choice depends upon the flow. Our numerical experiments show that the best choice is the horizontal velocity for the Kelvin-Helmholtz flow. This is agreement with Ref.[5]. There is no very strong gradient in the Rayleigh-Bénard convection, as a result, all variables, except the density, lead to the Gauss-Lobatto mesh.

## 4 Numerical results

### 4.1 The Rayleigh-Bénard instability

We first simulated the Rayleigh-Bénard convection as a test of the domain decomposition method since there is no strong gradients in this flow. The fluid layer is extending from  $z_0$  to  $z_0 + d$ , where  $z_0$  is the altitude and  $d$  the layer

thickness. The vertical  $z$  axis is directed downwards so that the gravitation represented by the vector  $\mathbf{g} = (0, g)$  is positive along this direction. The equations are classically written under a dimensionless form by using  $d$  as the unit of length so that the fluid extends from  $Z^{-1}$  to  $Z^{-1} + 1$ , where  $Z = d/z_0$ . The units of density and temperature are the values at the top of the layer,  $\rho(z_0)$  and  $T(z_0)$ , respectively. The unit of time is given by the viscous time scale  $d^2\rho(z_0)/\mu$ , where  $\mu$  is the constant dynamic viscosity. Moreover, we choose a zero temperature at the origin so that the basic conduction state, obtained by canceling  $\partial/\partial t$  and the two components of the velocity  $u$  and  $v$  in the Navier-Stokes equations, reads [15]

$$(15) \quad T_o(z) = zZ, \quad \rho_o(z) = [zZ]^m,$$

where  $m$  is the polytropic index. The equation of state is the perfect gas law. The constants introduced in Eqs.(1-4) are expressed as

$$(16) \quad \begin{aligned} A_u &= \mathcal{R}/\left(\sigma(m+1)^2 Z^2 \left[\frac{1}{m+1} - \frac{\gamma-1}{\gamma}\right]\right), \\ B_u &= 1, C_{u_1} = 0, C_{u_2} = A_u(Z(m+1)), \\ A_T &= A_u, B_T = A_u\gamma/(\gamma-1)\sigma, C_T = 1. \end{aligned}$$

where  $\mathcal{R}$  is the Rayleigh number, the Prandtl number is  $\sigma$  and  $\gamma$  is the adiabatic index. The boundary conditions are of Neumann type for the velocity and of Dirichlet type for the temperature.

$$(17) \quad \begin{aligned} v = 0, \partial_z u = 0 &\quad \text{on } z = Z^{-1}, Z^{-1} + 1 \\ T = 1, Z + 1 &\quad \text{on } z = Z^{-1}, Z^{-1} + 1 \end{aligned}$$

A steady solution characterized by a Rayleigh number equal to 1000,  $Z = 1$ ,  $m = 1$ , a Prandtl number and the adiabatic index equal to 0.71 and 1.67 respectively, has been computed. This solution has also been obtained with a single domain pseudo-spectral code [20] and it is used here as a test of the multidomain method. The mesh is made of two subdomains, the interface is located at  $z = 1.5$ , 26 Chebyshev polynomials and 32 Fourier functions have been used in each subdomain. Some characteristics of the solution are given in Table 1. The differences

between the multi and single-domain are very small. This solution has been obtained for three values of the tolerance of resolution of the elliptic problems :  $10^{-8}$ ,  $10^{-10}$  and  $10^{-12}$ . The formula (5) is mainly used with  $\eta = 1$ . However, the choice  $\eta = 0.5$  has been tested and does not affect this steady state.

This solution has also been obtained with 2 domains and the interface located at  $z = 1.67$ . In this case, 37 and 17 Chebyshev polynomials with 32 Fourier functions have been used in each domain. In all cases, the matchings of the functions are exact. The error on the first derivatives across the interface is defined as

$$ER[u'] = \left\| \frac{u'_s(z_{t,s}) - u'_{s+1}(z_{b,s+1})}{u'_s(z_{t,s}) + u'_{s+1}(z_{b,s+1})} \right\|, s = 1, \dots, S-1. \quad (18)$$

This quantity is of the order of  $10^{-10}$  for the velocity and the temperature. We have checked that spectral accuracy has been reached by looking at the decay of the coefficient of the expansions in the Chebyshev-Fourier space. The vorticity contours of this steady convection are shown in

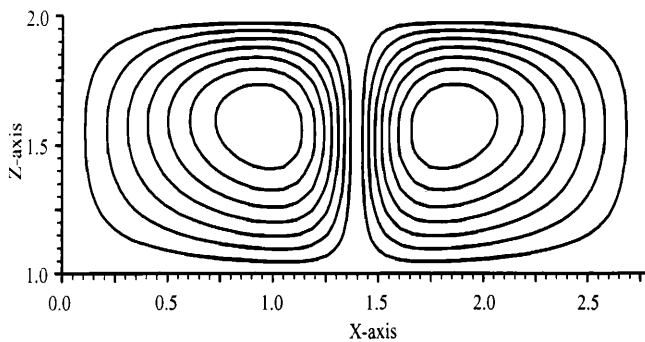


Figure 1: Contours of the vorticity in the Rayleigh-Bénard flow.

Fig. 1 and contours of the divergence are in Fig. 2. Note the smooth contours of these quantities, obtained by derivation of the primitive variables.

In these steady solutions, matchings of the second derivatives of the velocity and temperature are very good. It depends on the tolerance of resolution of the elliptic problems defined by Eqs.(8-12). For a tolerance of  $10^{-8}$ , the accuracy is of the order of  $10^{-2}$ ; for a tolerance of  $10^{-12}$ , the errors are only of  $10^{-5} - 10^{-6}$ .

## 4.2 The Kelvin-Helmholtz instability

This flow has received much attention in the last years, due to its application in Scramjet conception. Direct numerical simulations have been carried out using either finite-difference type method and spectral methods [5]. The

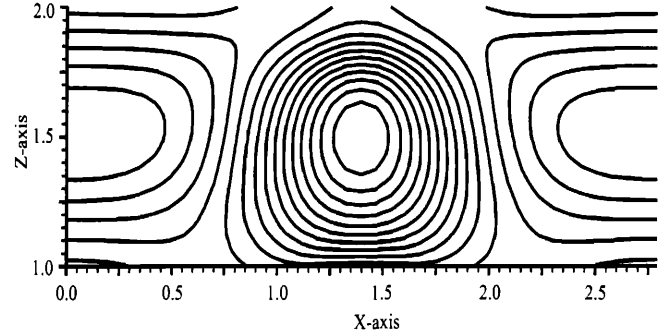


Figure 2: Contours of the divergence in the Rayleigh-Bénard flow.

method used in this reference has been detailed in the introduction. It is based on a Chebyshev expansion in the two directions and an adaptive mapping in the vertical direction. The domain decomposition method described previously has been run on this configuration. We present in this section some simulations of this flow. From a numerical point of view, the interest comes from the presence of large gradients of horizontal velocity in addition with the unsteady character of this configuration. The basic state is found by assuming, as in the boundary layer approximation, that the pressure is constant and the total enthalpy is constant with the Prandtl number is equal to one.

$$u = \frac{1}{2} \text{Tanh}(2z), \quad v = 0, \quad (19)$$

$$T = 1 + \frac{\gamma - 1}{2} M^2 (1 - 4u^2),$$

$$A_u = \frac{1}{4\gamma M^2}, \quad B_u = \frac{1}{Re}, \quad C_{u_i} = 0. \quad (20)$$

$$A_T = \frac{(\gamma - 1)}{\gamma}, \quad B_T = \frac{1}{Re\sigma}, \quad C_T = 4(\gamma - 1) \frac{M^2}{Re}.$$

Regarding the boundary conditions, both the horizontal velocity and the temperature are of Neumann type

$$v = 0, \quad \partial_z u = 0, \quad \partial_z T = 0 \quad \text{on } z = z_{b,1}, z_{t,S}. \quad (21)$$

The code has been run on a Kelvin-Helmholtz flow defined by a Reynolds number equal to 400, a Mach number equal to 0.8 and a wavelength of 20. The Prandtl number is 1 and the adiabatic index is 1.4. Three runs have been carried out with 3 subdomains with 72 Fourier functions and 51/51/51, 51/73/51, 91/51/91 Chebyshev polynomials. The interfaces are located at  $z = \pm 4$ . The matchings of the functions are exact. The error on the first derivatives, computed with the formula (18), is of the order of  $10^{-10}$  for the velocity. Since mappings are adapted

<i>Discretization</i>	$V_{max}$	$Mach_{max}$	$\rho_{max}$	$T_{max}$	$P_{max}$	$(\omega/\rho)_{max}$	$(\omega/\rho)_{min}$
51/51/51	0.64141	1.0695	0.32357	0.13266	0.35080	0.01072	-0.85754
51/73/51	0.64141	1.0691	0.32423	0.13343	0.35011	0.01089	-0.85762
91/51/91	0.64124	1.0692	0.32298	0.13245	0.35000	0.01023	-0.85763

Table 2: Characteristics of the time dependent Kelvin-Helmholtz solution, at  $t = 40$ , computed on three domains. The interfaces are located at  $z = \pm 4$ . The Reynolds number and the Mach number are equal to 400 and 0.8 respectively. The wavelength of the initial perturbation is 20. The Prandtl number is 1 and the adiabatic index is 1.4. The potential vorticity is  $(\omega/\rho)$ .

on the horizontal component of the velocity, the error on the matching of the first derivative of the temperature is slightly larger: of the order of  $10^{-8}$ . The results of these three runs are very close to each other: notice that the meshes are not the same in these three test cases. This solution has been computed by [5] using their adaptive procedure on a single domain. The comparison is performed by looking at the evolution of global quantities, such as the vorticity thickness, and some characteristics of the solution reported in Table 2. The vorticity thickness is defined as [5]

$$(22) \quad \delta_{\omega}^{-1} = \delta_i^{-1} \frac{\partial}{\partial z} \left( \frac{\overline{\rho u}}{\bar{\rho}} \right) \Big|_{max},$$

where the overbar denotes the average in the  $x$ -direction. Its evolution is represented in Fig.3 and is in very good agreement with the thickness reported in [5]. The vorticity contours of this unsteady solution are represented in Fig. 4 and contours of the divergence are displayed in Fig. 5. The importance of the velocity gradients are revealed in Fig. 6. These gradients justify the use of both domain decomposition and self-adaptive coordinate transformations.

In these time-dependent simulations, especially when the spatial resolution is not high enough, the second derivatives deteriorate as time goes on. However, in the results presented in the paper, the errors remain acceptable.

## 5 Conclusions

One of the first examples of domain decomposition, associated with a self-adaptive coordinate transformation, for the numerical solution of the viscous compressible flow simulations has been described. Numerical applications to stationary and time-dependent two-dimensional viscous compressible flows have been carried out.

One of the difficulties is that the number of mesh points has to be large enough to ensure accurate derivatives at the interfaces. In this way, the coefficients of the influence matrix are precisely computed. As the solution becomes stiff,

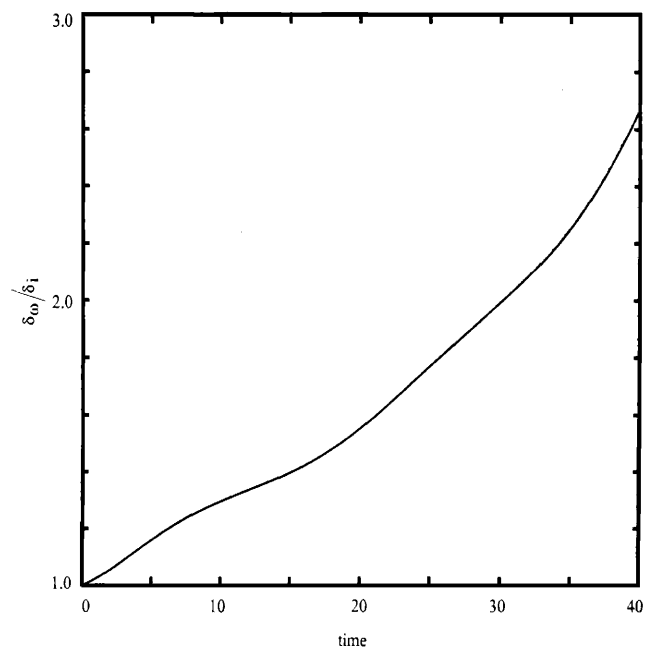


Figure 3: Evolution of the vorticity thickness in the Kelvin-Helmholtz flow.

the number of mesh points needed can be very large. An approximate solution of the influence matrix linear system and the equations of the continuity of the second derivatives, might be a way to overcome this difficulty.

The extension to three-dimensional flows with two homogeneous directions is straightforward. Generalization to multiple non-periodic directions is also possible.

## 6 Acknowledgments

We wish to thank R. Peyret for helpful comments and suggestions. We also thank H. Guillard and J.M. Malé for having provided to us the software of the adaptive procedure.

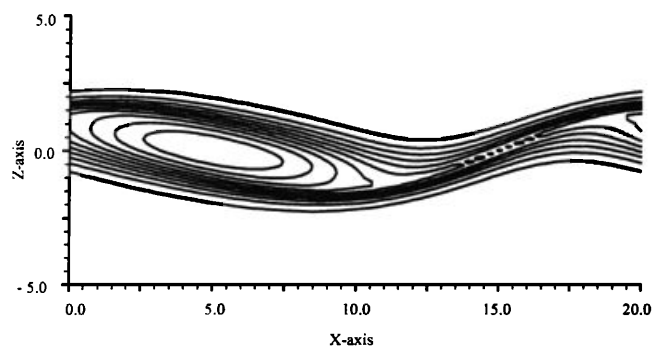


Figure 4: Contours of the vorticity in the Kelvin-Helmholtz flow at  $t = 40$ .

## References

- [1] A. Quarteroni, J. Periaux, Y. A. Kuznetsov and O. B. Widlund, *Domain Decomposition Methods in Science and Engineering*, AMS, Providence 1994.
- [2] A. Bayliss and B. J. Matkowsky, *Fronts, Relaxation Oscillations, and Period Doubling in Solid Fuel Combustion*, J. Comp. Phys., 71, (1987), pp. 147-168.
- [3] H. Guillard and R. Peyret, *On the Use of Spectral Methods for the Numerical Solution of Stiff Problems*. Comput. Methods Appl. Mech. Eng., 66, (1988), pp.17-43.
- [4] J. M. Augenbaum, *An Adaptive Pseudo-Spectral Method for Discontinuous Problems*, Appl. Numer. Math. 5 (1989) pp. 459-480.
- [5] H. Guillard, J. M. Malé and R. Peyret, *Adaptive Spectral Methods with Application to Mixing Layer Computations*, J. Comput. Phys., 102 (1992), pp. 114-127.
- [6] J.M. Malé, *Calcul d'écoulements visqueux compressibles par méthodes spectrales auto-adaptatives. Application aux couches de mélange*. Thèse Université de Nice-Sophia Antipolis, 1992.
- [7] A. Bayliss, D. Gottlieb, B. J. Matkowsky and M. Minkoff, *An Adaptive Pseudo-Spectral Method for Reaction Diffusion Problems*, J. Comput. Phys., 81 (1989), pp421-443.
- [8] A. T. Patera, *A Spectral Element Method for Fluid Dynamics: Laminar Flow in a Channel Expansion*, J. Comput. Phys., 54 (1984), pp. 468-488.
- [9] C. R. Schneidesh and M. O. Deville, *Chebyshev Collocation Method and Multi-domain Decomposition for Navier-Stokes Equations in Complex Curved Geometries*, J. Comput. Phys., 106 (1993), pp. 234-257.
- [10] M. G. Macaraeg and C. L. Streett, *A Spectral Multi-Domain Technique for Viscous Compressible Reacting Flows*, 8 (1988), pp.1121-1134.
- [11] D. A. Kopriva, *Computation of Hyperbolic Equations on Complicated Domains with Patched and Overset Chebyshev Grids*, SIAM J. Sci. Stat. Comput., 10 (1989), pp. 120-132.
- [12] D. A. Kopriva, *Multidomain Spectral Solution of Compressible Viscous Flows*, J. Comp. Phys., 115 (1994), pp. 184-199.
- [13] C. Canuto, M. Y. Hussaini, A. Quarteroni and T. A. Zang, *Spectral Methods in Fluids Dynamics*, Springer-Verlag, 1988.
- [14] J. H. Williamson, *Low Storage Runge-Kutta Schemes*, J. Comp. Phys., 35 (1980), pp. 48-56.
- [15] S. Gauthier, *A Semi-Implicit Collocation Method: Application to Thermal Convection in 2D Compressible Fluids*, Num. Meth. in Fluids Dynamics, 12 (1991), pp. 985-1002.

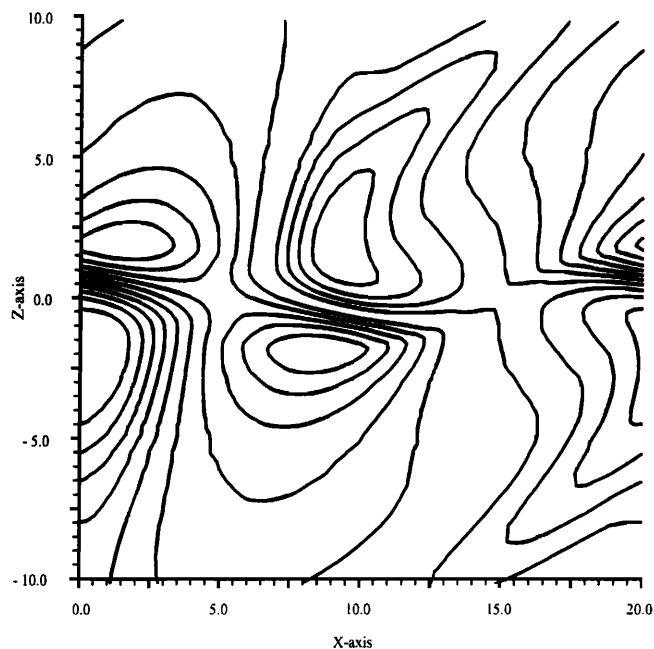


Figure 5: Contours of the divergence in the Kelvin-Helmholtz flow at  $t = 40$ .

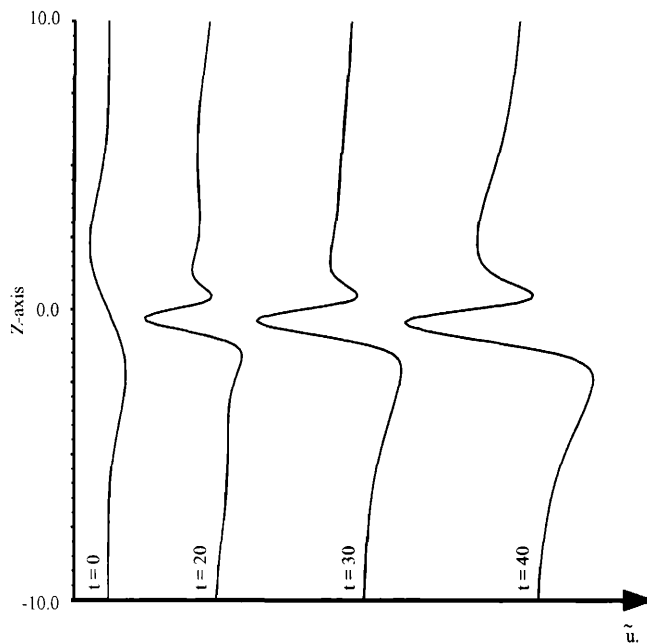


Figure 6: Profiles of the horizontal velocity fluctuation versus  $z$ . in the Kelvin-Helmholtz flow, at different times.

- [16] J.P. Pulicani, *A Spectral Multi-Domain Method for the Solution of 1D- Helmholtz and Stokes-Type Equations*, Computers and Fluids, 16 (1988 ) pp. 207-215.
- [17] J. M. Lacroix, R. Peyret and J.P. Pulicani, *A Pseudo-Spectral Multi-Domain Method for the Navier-Stokes Equations with Application to Double-Diffusive Convection*, in Proc. Seventh GAMM Conf. Numer. Math. Fluid Mech., M. Deville, Ed., pp. 167-174, Vieweg, Braunschweig 1988.
- [18] D. Gottlieb and S. A. Orszag, *Numerical Analysis of Spectral Methods: Theory and Applications*, SIAM, Philadelphia 1977.
- [19] T. Passot and A. Pouquet, *Numerical Simulations of Three- Dimensional Supersonic Flows*, Eur. J. Mech., B/Fluids, 10 (1991), pp 377-394.
- [20] S. Gauthier, *A Spectral Collocation Method for Two-Dimensional Compressible Convection*, J. Comp. Phys., 75 (1988), pp. 217-235.